

¹ Functional MRI brain state ² occupancy in the presence of ³ cerebral small vessel disease – a ⁴ pre-registered replication analysis of ⁵ the Hamburg City Health Study

✉ For correspondence:

e.schlemm@uke.de

Present address:

Dr. Dr. Eckhard Schlemm,
Klinik und Poliklinik für
Neurologie,
Universitätsklinikum
Hamburg-Eppendorf,
Martinistr. 52,
D-20251 Hamburg

Data availability:

Preprocessed data will be
available e.g. on
<https://github.com/csi-hamburg/HCHS-brain-states-RR>.

Funding: Deutsche
Forschungsgemeinschaft
(DFG) – SFB 936,
178316478 – C2 (Drs
Thomalla & Cheng)

Competing interests: The
authors declare no
competing interests.

⁶ Thies Ingwersen, MD  ¹, Carola Mayer, PhD ¹, Marvin Petersen, MD ¹,
⁷ Benedikt M. Frey, MD ¹, Jens Fiehler, MD ², Uta Hanning, MD ²,
⁸ Simone Kühn, PhD ^{3,4}, Jürgen Gallinat, MD ³, Raphael Twerenbold,
⁹ MD ⁵, Christian Gerloff, MD ⁶, Bastian Cheng, MD  ¹, Götz Thomalla,
¹⁰ MD ¹, Eckhard Schlemm, MBBS PhD  

¹¹ Department of Neurology, University Medical Center

¹² Hamburg-Eppendorf; ²Department of Neuroradiology, University

¹³ Medical Center Hamburg-Eppendorf; ³Department of Psychiatry,

¹⁴ University Medical Center Hamburg-Eppendorf; ⁴Max-Planck-Institut für

¹⁵ Bildungsforschung, Berlin; ⁵Department of Cardiology, University

¹⁶ Medical Center Hamburg-Eppendorf; ⁶University Medical Center

¹⁷ Hamburg-Eppendorf

¹⁸

¹⁹ Abstract

²⁰ **Objective:** To replicate recent findings on the association between the extent of
²¹ cerebral small vessel disease (cSVD), functional brain network dedifferentiation, and
²² cognitive impairment.

²³ **Methods:** We analyzed demographic, imaging, and behavioral data from the

²⁴ prospective population-based Hamburg City Health Study. Using a fully prespecified
²⁵ analysis pipeline, we estimated discrete brain states from structural and resting-state
²⁶ functional magnetic resonance imaging (MRI). In a multiverse analysis, we varied brain
²⁷ parcellations and functional MRI confound regression strategies. The severity of cSVD
²⁸ was operationalized as the volume of white matter hyperintensities of presumed
²⁹ vascular origin. Processing speed and executive dysfunction were quantified using the
³⁰ Trail Making Test (TMT).

³¹ **Hypotheses:** We hypothesized a) that a greater volume of supratentorial white matter
³² hyperintensities would be associated with less time spent in functional MRI-derived
³³ brain states of high fractional occupancy; and b) that less time spent in these
³⁴ high-occupancy brain states is associated with a longer time to completion in part B of
³⁵ the TMT.

³⁶ **Results:** High-occupancy brain states were characterized by activation or suppression
³⁷ of the default mode network. Every 5.1-fold increase in WMH volume was associated
³⁸ with a 0.94-fold reduction in the odds of occupying DMN-related brain states (P
³⁹ 5.01×10^{-8}). Every 5 % increase in time spent in high-occupancy brain states was
⁴⁰ associated with a 0.98-fold reduction in the TMT-B completion time (P 0.0116). Findings
⁴¹ were robust across most brain parcellations and confound regression strategies.

⁴² **Conclusion:** We successfully replicated previous findings on the association between
⁴³ cSVD, functional brain occupancy, and cognition in an independent sample. The data
⁴⁴ provide further evidence for a functional network dedifferentiation hypothesis of
⁴⁵ cSVD-related cognitive impairment. Further research is required to elucidate the
⁴⁶ mechanisms underlying these associations.

⁴⁷ —————

⁴⁸ Introduction

⁴⁹ Cerebral small vessel disease (cSVD) is an arteriolopathy of the brain associated with age
⁵⁰ and common cardiovascular risk factors (Wardlaw, C. Smith, and Dichgans, 2013). cSVD
⁵¹ predisposes patients to ischemic stroke (in particular lacunar stroke) and may lead to
⁵² cognitive impairment and dementia (Cannistraro et al., 2019). Neuroimaging findings in
⁵³ cSVD reflect its underlying pathology (Wardlaw, Valdés Hernández, and Muñoz-Maniega,
⁵⁴ 2015) and include white matter hyperintensities (WMH), lacunes of presumed vascular
⁵⁵ origin, small subcortical infarcts and microbleeds, enlarged perivascular spaces as well

56 as brain atrophy (Wardlaw, E. E. Smith, et al., 2013). However, the extent of visible cSVD
57 features on magnetic resonance imaging (MRI) is an imperfect predictor of the severity
58 of clinical sequelae (Das et al., 2019) and our understanding of the causal mechanisms
59 linking cSVD-associated brain damage to clinical deficits remains limited (Bos et al., 2018).
60 Recent efforts have focused on exploiting network aspects of the structural (Tuladhar,
61 Dijk, et al., 2016; Tuladhar, Tay, et al., 2020; Lawrence, Zeestraten, et al., 2018) and func-
62 tional (Dey et al., 2016; Schulz et al., 2021) organization of the brain to understand the
63 relationship between cSVD and clinical deficits in cognition and other domains that rely
64 on distributed processing. Reduced structural network efficiency has repeatedly been
65 described as a causal factor in the development of cognitive impairment, particularly
66 executive dysfunction and reduced processing speed in cSVD (Lawrence, Chung, et al.,
67 2014; Shen et al., 2020; Reijmer et al., 2016; Prins et al., 2005). Findings with respect
68 to functional connectivity (FC), however, are more heterogeneous than their SC counter-
69 parts, perhaps because FC measurements are prone to be affected by hemodynamic
70 factors and noise, resulting in relatively low reliability, especially with resting-state scans
71 of short duration (Laumann, Gordon, et al., 2015). This problem is exacerbated in the
72 presence of cSVD and worsened by arbitrary processing choices (Lawrence, Tozer, et al.,
73 2018; Gesierich et al., 2020).

74 As a promising new avenue, time-varying, or dynamic, functional connectivity approaches
75 have recently been explored in patients with subcortical ischemic vascular disease (Yin et
76 al., 2022; Xu et al., 2021). Although the study of dynamic FC measures may not solve the
77 problem of limited reliability, especially in small populations or subjects with extensive
78 structural brain changes, it adds another – temporal – dimension to the study of func-
79 tional brain organization, which is otherwise overlooked. Importantly, FC dynamics not
80 only reflect moment-to-moment fluctuations in cognitive processes, but are also related
81 to brain plasticity and homeostasis (Laumann and Snyder, 2021; Laumann, Snyder, et al.,
82 2017), which may be impaired in cSVD.

83 In the present paper, we aimed to replicate and extend the main results of (Schlemm
84 et al., 2022). In this recent study, the authors analyzed MR imaging and clinical data from
85 the prospective Hamburg City Health Study (HCHS, (Jagodzinski et al., 2020)) using a coac-
86 tivation pattern approach to define discrete brain states and found associations between
87 the WMH load, time spent in high-occupancy brain states characterized by activation or
88 suppression of the default mode network (DMN), and cognitive impairment. Specifically,

89 every 4.7-fold increase in WMH volume was associated with a 0.95-fold reduction in the
90 odds of occupying a DMN-related brain state; every 2.5 seconds (i.e., one repetition time)
91 not spent in one of those states was associated with a 1.06-fold increase in TMT-B com-
92 pletion times.

93 The fractional occupancy of a functional MRI-derived discrete brain state is a subject-
94 specific measure of brain dynamics and is defined as the proportion of BOLD volumes
95 assigned to that state relative to all BOLD volumes acquired during a resting-state scan.

96 Our primary hypothesis for the present work was that the volume of supratentorial
97 white matter hyperintensities is associated with fractional occupancy of DMN-related
98 brain states in a middle-aged to elderly population mildly affected by cSVD. Our sec-
99 ondary hypothesis was that fractional occupancy is associated with executive dysfunc-
100 tion and reduced processing speed, measured as the time to complete part B of the Trail
101 Making Test (TMT).

102 Both hypotheses were tested in an independent subsample of the HCHS study popu-
103 lation using the same imaging protocols, examination procedures, and analysis pipelines
104 as those in (Schlemm et al., 2022). The robustness of the associations was explored using
105 a multiverse approach by varying key steps in the analysis pipeline.

106 Methods

107 Study population

108 This study analyzed data from the Hamburg City Health Study (HCHS), an ongoing prospec-
109 tive, population-based cohort study aiming to recruit a cross-sectional sample of 45 000
110 adult participants from the city of Hamburg, Germany (Jagodzinski et al., 2020). From
111 the first 10 000 participants of the HCHS, we planned to include those who were docu-
112 mented to have received brain imaging (n=2648) and exclude those who were analyzed
113 in our previous report (Schlemm et al., 2022) (n=970). The ethical review board of the
114 Landesärztekammer Hamburg (State of Hamburg Chamber of Medical Practitioners) ap-
115 proved the HCHS (PV5131), and all participants provided written informed consent.

116 Demographic and clinical characterization

117 From the study database, we extracted the participants' age at the time of inclusion in
118 years, their sex, and the number of years spent in education. During the visit to the study
119 center, participants underwent cognitive assessment using standardized tests. From the

¹²⁰ database, we extracted their performance scores on the Trail Making Test part B, mea-
¹²¹ sured in seconds, as an operationalization of executive function and psychomotor pro-
¹²² cessing speed (Tombaugh, 2004; Arbuthnott and Frank, 2000). For descriptive purposes,
¹²³ we also extracted data on past medical history and reported the proportion of partici-
¹²⁴ pants with a previous diagnosis of dementia.

¹²⁵ **MRI acquisition and preprocessing**

¹²⁶ The magnetic resonance imaging protocol for the HCHS includes structural and resting-
¹²⁷ state functional sequences. The acquisition parameters for a 3 T Siemens Skyra MRI scan-
¹²⁸ ner (Siemens, Erlangen, Germany) have been previously reported (Petersen et al., 2020;
¹²⁹ Frey et al., 2021) and are given as follows:

¹³⁰ For T_1 -weighted anatomical images, a 3D rapid acquisition gradient-echo sequence
¹³¹ (MPRAGE) was used with the following sequence parameters: repetition time TR = 2500 ms,
¹³² echo time TE = 2.12 ms, 256 axial slices, slice thickness ST = 0.94 mm, and in-plane resolu-
¹³³ tion IPR = $(0.83 \times 0.83) \text{ mm}^2$.

¹³⁴ T_2 -weighted fluid attenuated inversion recovery (FLAIR) images were acquired with
¹³⁵ the following sequence parameters: TR = 4700 ms, TE = 392 ms, 192 axial slices, ST =
¹³⁶ 0.9 mm, IPR = $(0.75 \times 0.75) \text{ mm}^2$.

¹³⁷ 125 resting state functional MRI volumes were acquired (TR = 2500 ms; TE = 25 ms;
¹³⁸ flip angle = 90°; slices = 49; ST = 3 mm; slice gap = 0 mm; IPR = $(2.66 \times 2.66) \text{ mm}^2$). The
¹³⁹ subjects were asked to keep their eyes open and to think of nothing.

¹⁴⁰ We verified the presence and voxel dimensions of expected MRI data for each par-
¹⁴¹ ticipant and excluded those for whom at least one of T_1 -weighted, FLAIR, and resting-
¹⁴² state MRI was missing. We also excluded participants with neuroradiologically confirmed
¹⁴³ space-occupying intra-axial lesion. To ensure reproducibility, no visual quality assess-
¹⁴⁴ ment of raw images was performed.

¹⁴⁵ For the remaining participants, structural and resting-state functional MRI data was
¹⁴⁶ preprocessed using FreeSurfer v6.0 (<https://surfer.nmr.mgh.harvard.edu/>), and fmriPrep
¹⁴⁷ v20.2.6 (Esteban et al., 2019), using default parameters. Participants were excluded if
¹⁴⁸ automated processing using at least one of these packages failed.

¹⁴⁹ **Quantification of WMH load**

¹⁵⁰ For our primary analysis, the extent of ischemic white matter disease was operational-
¹⁵¹ ized as the total volume of supratentorial WMHs obtained from automated segmentation

152 using a combination of anatomical priors, BIANCA (Griffanti, Zamboni, et al., 2016), and
153 LOCATE (Sundaresan et al., 2019), post-processed with a minimum cluster size of 30 vox-
154 els, as described in (Schlemm et al., 2022). In an exploratory analysis, we partitioned
155 voxels identified as WMH into deep and periventricular components according to their
156 distance to the ventricular system (cut-off 10 mm, (Griffanti, Jenkinson, et al., 2018))

157 **Brain state estimation**

158 The output from fMRIprep was post-processed using xcpEngine v1.2.1 to obtain de-confounded
159 spatially averaged BOLD time series (Circi, Wolf, et al., 2017). For the primary analysis, we
160 used the $36p$ regression strategy and the Schaefer-400 parcellation (Schaefer et al., 2018),
161 as in (Schlemm et al., 2022).

162 Different atlases and confound regression strategies, as implemented in xcpEngine,
163 were included in an exploratory multiverse analysis.

164 Co-activation pattern (CAP) analysis was performed by first aggregating parcellated,
165 de-confounded BOLD signals into a ($n_{\text{parcels}} \times \sum_i n_{\text{time points},i}$) feature matrix, where $n_{\text{time points},i}$
166 denotes the number of retained volumes for subject i after confound regression. Clus-
167 tering was performed using the k -means algorithm ($k = 5$) with a distance measure given
168 by 1 minus the sample Pearson correlation between points, as implemented in Matlab
169 R2021a. We estimated the subject- and state-specific fractional occupancies, which are
170 defined as the proportion of BOLD volumes assigned to each brain state (Vidaurre et al.,
171 2018). The two states with the highest average occupancies were identified as the basis
172 for further analysis.

173 **Statistical analysis**

174 For demographic (age, sex, and years of education) and clinical (TMT-B) variables, the
175 number of missing items is reported. For non-missing values, we provide descriptive
176 summary statistics using median and interquartile range. The proportions of men and
177 women in the sample are reported. Since we expected based on our pilot data (Schlemm
178 et al., 2022) that the proportion of missing data would be small, primary regression mod-
179elling was carried out as a complete-case analysis.

180 As an outcome-neutral quality check of the implementation of the MRI processing
181 pipeline, brain state estimation, and co-activation pattern analysis, we compared frac-
182 tional occupancies between brain states. We expected that the average fractional oc-
183 cupancy in the two high-occupancy states would be higher than the average fractional

¹⁸⁴ occupancy in the other three states. Point estimates and 95% confidence intervals are
¹⁸⁵ presented for the difference in average fractional occupancy to verify this assertion.

¹⁸⁶ For further analyses, non-zero WMH volumes were subjected to logarithmic transfor-
¹⁸⁷ mation. Zero values retained their value of zero; to compensate, all models included a
¹⁸⁸ binary indicator for zero WMH volume if at least one non-zero WMH value was present.

¹⁸⁹ To assess the primary hypothesis of a negative association between the extent of
¹⁹⁰ ischemic white matter disease and time spent in high-occupancy brain states, we per-
¹⁹¹ formed a fixed-dispersion Beta regression to model the logit of the conditional expec-
¹⁹² tation of the average fractional occupancy of two high-occupancy states as an affine
¹⁹³ function of the logarithmized WMH load. Age and sex were included as covariates. The
¹⁹⁴ strength of the association was quantified as the odds ratio per interquartile ratio of the
¹⁹⁵ WMH burden distribution, and is accompanied by a 95% confidence interval. Significance
¹⁹⁶ testing of the null hypothesis of no association was conducted at the conventional signif-
¹⁹⁷ icance level of 0.05. Estimation and testing were carried out using the 'betareg' package
¹⁹⁸ v3.1.4 in R v4.2.1.

¹⁹⁹ To assess the secondary hypothesis of an association between time spent in high-
²⁰⁰ occupancy brain states and executive dysfunction, we performed a generalized linear
²⁰¹ regression with a Gamma response distribution to model the logarithm of the condi-
²⁰² tional expected completion time in part B of the TMT as an affine function of the average
²⁰³ fractional occupancy of two high-occupancy states. Age, sex, years of education, and
²⁰⁴ logarithmized WMH load were included as covariates. The strength of the association
²⁰⁵ was quantified as a multiplicative factor per percentage point and accompanied by a
²⁰⁶ 95% confidence interval. Significance testing of the null hypothesis of no association was
²⁰⁷ conducted at the conventional significance level of 0.05. Estimation and testing were
²⁰⁸ performed using the glm function included in the 'stats' package from R v4.2.1.

²⁰⁹ Pre-registered analyses

²¹⁰ The analysis plan was pre-registered on June 27 2023 at <https://osf.io/fcqmb>. The sample
²¹¹ size calculation was based on an effect size on the odds ratio scale of 0.95, correspond-
²¹² ing to an absolute difference in the probability of occupying a DMN-related brain state
²¹³ between the first and third WMH-load quartile of 1.3 percentage points, and between
²¹⁴ the 5% and 95% percentile of 3.1 percentage points. Approximating half the difference
²¹⁵ in fractional occupancy of DMN-related states between different task demands (rest vs n-
²¹⁶ back) in healthy subjects, which was estimated to lie between 6 and 7 percentage points

²¹⁷ (Cornblath et al., 2020), this value represented a plausible choice for the smallest effect
²¹⁸ size of theoretical and practical interest. It also equals the estimated effect size based on
²¹⁹ the data presented in (Schlemm et al., 2022).

²²⁰ Simple bootstrapping was used to create 10 000 hypothetical datasets of size 200, 400,
²²¹ 600, 800, 900, 910, ..., 1090, 1100, 1200, 1400, 1500, and 1600. Each dataset was then sub-
²²² jected to the estimation procedure described above. For each sample size, the propor-
²²³ tion of datasets in which the primary null hypothesis of no association between fractional
²²⁴ occupancy and WMH load could be rejected at $\alpha = 0.05$ was computed and recorded as
²²⁵ a power curve in Figure 1.

²²⁶ A sample size of 960 would have allowed the replication of the reported effect with a
²²⁷ power of 80.2 %. We had anticipated a sample size of 1500, which would have yielded a
²²⁸ power of 93.9 %.

²²⁹ Multiverse analysis

²³⁰ In both (Schlemm et al., 2022) and our primary replication analysis, we made certain ana-
²³¹ lytical choices in the operationalization of brain states and ischemic white matter disease,
²³² namely the use of the 36*p* confound regression strategy, the Schaefer-400 parcellation,
²³³ and a BIANCA/LOCATE-based WMH segmentation algorithm. The robustness of the as-
²³⁴ sociation between WMH burden and time spent in high-occupancy states with regard to
²³⁵ other choices was explored in a multiverse analysis (Steegen et al., 2016). Specifically, in
²³⁶ an exploratory analysis, we estimated brain states from BOLD time series processed ac-
²³⁷ cording to a variety of established confound regression strategies and aggregated over
²³⁸ different cortical brain parcellations (Table 2, Ceric, Rosen, et al., 2018; Ceric, Wolf, et al.,
²³⁹ 2017). The extent of cSVD was additionally quantified by the volume of deep and periven-
²⁴⁰ tricular white matter hyperintensities.

²⁴¹ For each combination of analytical choice of confound regression strategy, parcella-
²⁴² tion, and subdivision of white matter lesion load ($9 \times 9 \times 3 = 243$ scenarios in total), we
²⁴³ quantified the association between WMH load and average time spent in high-occupancy
²⁴⁴ brain states using odds ratios and 95 % confidence intervals as described above.

²⁴⁵ No hypothesis testing was performed for these multiverse analyses. Rather, they
²⁴⁶ serve to inform about the robustness of the outcome of the test of the primary hypoth-
²⁴⁷ esis. Any substantial conclusions about the association between the severity of cerebral
²⁴⁸ small vessel pathology and the time spent in high-occupancy brain states were drawn
²⁴⁹ from the primary analysis using pre-specified methodological choices, as stated in the

250 Scientific Question in Table 1.

251 **Further exploratory analysis**

252 In previous work, two high-occupancy brain states have been related to the default mode
253 network (Cornblath et al., 2020). We further explored this relationship by computing, for
254 each individual brain state, the cosine similarity of the positive and negative activations of
255 the cluster's centroid with a set of a priori defined functional 'communities' or networks
256 (Schaefer et al., 2018; Yeo et al., 2011). The results were visualized as spider plots for the
257 Schaefer atlases.

258 In further exploratory analyses, we describe the associations between brain state dy-
259 namics and other measures of cognitive ability such as memory and language.

260 **Results**

261 For this replication study, a total of 2648 datasets were available, of which 970 were al-
262 ready included in our previous analysis and thus discarded. In 13 of the resulting 1678
263 datasets, one or more MRI sequences were missing. Of the complete datasets (n=1665),
264 we excluded 5 participants due to intra-axial space-occupying lesions. An additional 9
265 subjects were excluded because of unsuccessful preprocessing, WMH segmentation, or
266 xcpEngine failure, resulting in 1651 datasets for analysis. A study-flowchart is provided in
267 Figure 2.

268 Baseline demographic and cognitive values, including the number of missing items,
269 are reported in Table 4.

270 WMH volumes (median 1.05 mL, IQR 0.47 mL to 2.37 mL), motion estimates, and frac-
271 tional occupancies of brain states 1 through 5 are reported in Table 6.

272 In an outcome-neutral quality check of the implementation of (i) the MRI processing
273 pipeline, (ii) brain state estimation, and (iii) co-activation pattern analysis, the mean dif-
274 ference in fractional occupancy between high- and low-occupancy states was significant,
275 with a point-estimate of 6.7 % and a 95 % confidence interval of 6.2 % to 7.1 %. This indicates
276 that the implementation of the pipeline was correct and that the brain state estimation
277 and co-activation pattern analysis worked as intended.

278 Pre-registered hypotheses

279 Association between WMH load and fractional occupancy

280 The results of the test of our primary preregistered hypothesis of an association be-
281 tween supratentorial WMH volume and the time spent in high-occupancy brain states
282 are shown in Figure 3 and Table 8.

283 Adjusted for age and sex, there was a 0.94-fold reduction in the odds of occupying a
284 high-occupancy brain state for every 5.1-fold increase in WMH load ($P 5.01 \times 10^{-8}$).

**285 Association between executive function and fractional occupancy in DMN-
286 related states**

287 The results of the test of our secondary preregistered hypothesis of an association be-
288 tween time spent in high-occupancy brain states and executive function as measured by
289 the complete part B of the TMT are shown in Figure 4 and Table 10.

290 Adjusted for age, sex, WMH volume, and years of education, there was a 0.98-fold
291 reduction in the time to complete the TMT-B for every 5 % increase in the time spent in
292 high-occupancy brain states ($P 0.0116$).

293 Multiverse analysis

294 In a multiverse analysis, the main findings of associations between WMH load and FO
295 and between FO and TMT-B were robust with respect to the processing choices of brain
296 parcellation and confound regression strategy.

297 A nominally statistically significant negative association between the total WMH load
298 and time spent in high-occupancy states was observed in 48/81 scenarios, with 8/81 sig-
299 nificant positive associations occurring with the Desikan–Killiany parcellation only (Fig-
300 ure 5A). For periventricular (deep) WMH volume, the results were similarly robust with
301 49/81 (39/81) negative and 8/81 (0/81) associations of nominal statistical significance, re-
302 spectively.

303 The secondary finding of an association between greater TMT-B times and lower frac-
304 tional occupancy was similarly robust with 16/81 nominally statistically significant neg-
305 ative and no significant positive associations, irrespective of operationalization of cSVD
306 (total vs. periventricular vs. deep WMH volume) (Figure 5B).

307 Additional analyses

308 Connectivity profiles of brain states – relation to default mode network
309 Based on the cosine similarity between positive and negative activations of cluster cen-
310 troids and indicator vectors of pre-defined large scale brain networks, network activation
311 profiles were computed for brain states estimated Schaefer parcellations of varying spa-
312 tial resolution.

313 Figure 6 shows the corresponding spider plots, identifying states characterized by
314 activation (DMN+) or suppression (DMN-) of the default mode network as states with the
315 highest fractional occupancy.

316 Association with wider cognitive domains

317 Associations between the time spent in high-occupancy DMN-related brain states and
318 cognitive measures beyond TMT-B are shown in Figure 7.

319 Adjusted for age, sex, WMH load, and years of education, FO appeared to be associ-
320 ated with word recall (aOR 2.4, nominal P 0.0153), but not with global cognitive function-
321 ing (MMSE, aOR 1.5), verbal fluency (animal naming, aOR 1.2), vocabulary (aOR 1.5), or
322 pure processing speed (TMT-A, aOR 0.87).

323 Summary and Discussion

324 In this pre-registered cross-sectional study we replicated the key findings of Schlemm
325 et al., 2022 in an independent population-based sample of 1651 middle-aged to elderly
326 participants of the Hamburg City Health Study.

327 First, we confirmed that the severity of cerebral small vessel disease is associated with
328 the time spent in high-occupancy brain states, defined by functional MRI. More precisely,
329 we showed that every 5.1-fold increase in the volume of supratentorial white matter hy-
330 perintensities of presumed vascular origin (WMH) was associated with a 0.95-fold reduc-
331 tion in the odds of occupying a brain state characterized by activation or suppression of
332 the default-mode network, at any given time during the resting-state scan.

333 Second, we confirmed that the time spent in high-occupancy brain states at rest is
334 associated with cognitive performance. More precisely, a 5%-reduction in the fractional
335 occupancy of DMN-related brain states was associated with a 1.02-fold increase in the
336 time to complete part B of the trail making test (TMT).

337 In a pre-planned multiverse analysis, these findings were robust with respect to vari-

338 ations in brain parcellations and confound regression strategies. Inconsistent results
339 were only found with the Desikan–Killiany parcellation irrespective of the confound re-
340 gression strategy, likely reflecting that the spatial resolution and functional specificity of
341 this coarse, structurally defined atlas are inadequate for analyzing functionally defined
342 brain states.

343 We also confirmed across several brain parcellation resolutions that high-occupancy
344 states at rest are characterized by either activation or suppression of the default mode
345 network, reflecting its role as the predominant task-negative brain network.

346 In unplanned, exploratory analyses, we described the association between brain state
347 dynamics and cognitive measures other than executive function and processing speed
348 and reported a strong, preliminary association between time spent in high-occupancy
349 states and delayed word recall.

350 We further explored, but did not report in detail, the effect of motion; all reported as-
351 sociations were robust to additional, unplanned adjustments for DVARS, RMSD or mean
352 framewise displacement.

353 The presented results provide robust evidence for a behaviorally relevant association
354 between cerebral small vessel disease and functional brain network dedifferentiation.

355 Further research is required to replicate our findings in different populations, such
356 as those affected more severely by cSVD or cognitive impairment, or being studied using
357 different imaging protocols, to determine the generalizability of our findings with respect
358 to varying operationalizations of the notions of cSVD, brain state, and cognition, and to
359 understand the mechanisms underlying the reported associations.

360 **Timeline and access to data**

361 At the time of planning of this study, all demographic, clinical and imaging data used in
362 this analysis had been collected by the HCHS and were held in the central trial database.
363 Quality checks for non-imaging variables had been performed centrally. WMH segmen-
364 tation based on structural MRI data of the first 10 000 participants of the HCHS had been
365 performed previously using the BIANCA/LOCATE approach (Rimmele et al., 2022). Func-
366 tional MRI data and clinical measures of executive dysfunction (TMT-B scores) had not
367 previously been analyzed by the pre-registering author (ES).

Acknowledgment

368 This preprint was created using the LaPreprint template (<https://github.com/roaldarbol/lapreprint>) by Mikkel Roald-Arbøl .

371 References

- 372** Arbuthnott, Katherine and Janis Frank (2000). "Trail making test, part B as a measure of
373 executive control: validation using a set-switching paradigm". In: *Journal of clinical and*
374 *experimental neuropsychology* 22.4, pp. 518–528.
- 375** Behzadi, Yashar et al. (2007). "A component based noise correction method (CompCor)
376 for BOLD and perfusion based fMRI". In: *Neuroimage* 37.1, pp. 90–101.
- 377** Bos, Daniel et al. (2018). "Cerebral small vessel disease and the risk of dementia: A sys-
378 tematic review and meta-analysis of population-based evidence". en. In: *Alzheimers.*
379 *Dement.* 14.11, pp. 1482–1492.
- 380** Cannistraro, Rocco J et al. (2019). "CNS small vessel disease: A clinical review". en. In: *Neu-*
381 *rology* 92.24, pp. 1146–1156.
- 382** Ceric, Rastko, Adon FG Rosen, et al. (2018). "Mitigating head motion artifact in functional
383 connectivity MRI". In: *Nature protocols* 13.12, pp. 2801–2826.
- 384** Ceric, Rastko, Daniel H Wolf, et al. (2017). "Benchmarking of participant-level confound
385 regression strategies for the control of motion artifact in studies of functional con-
386 nectivity". en. In: *Neuroimage* 154, pp. 174–187.
- 387** Cornblath, Eli J et al. (2020). "Temporal sequences of brain activity at rest are constrained
388 by white matter structure and modulated by cognitive demands". en. In: *Commun Biol*
389 3.1, p. 261.
- 390** Cox, Robert W (1996). "AFNI: software for analysis and visualization of functional mag-
391 netic resonance neuroimages". In: *Computers and Biomedical research* 29.3, pp. 162–
392 173.
- 393** Das, Alvin S et al. (2019). "Asymptomatic Cerebral Small Vessel Disease: Insights from
394 Population-Based Studies". en. In: *J. Stroke Cerebrovasc. Dis.* 21.2, pp. 121–138.
- 395** Desikan, Rahul S et al. (2006). "An automated labeling system for subdividing the human
396 cerebral cortex on MRI scans into gyral based regions of interest". In: *Neuroimage* 31.3,
397 pp. 968–980.
- 398** Dey, Ayan K et al. (2016). "Pathoconnectomics of cognitive impairment in small vessel
399 disease: A systematic review". en. In: *Alzheimers. Dement.* 12.7, pp. 831–845.

- ⁴⁰⁰ Esteban, Oscar et al. (2019). "fMRIprep: a robust preprocessing pipeline for functional
⁴⁰¹ MRI". en. In: *Nat. Methods* 16.1, pp. 111–116.
- ⁴⁰² Frey, Benedikt M et al. (2021). "White matter integrity and structural brain network topol-
⁴⁰³ ogy in cerebral small vessel disease: The Hamburg city health study". en. In: *Hum. Brain
404 Mapp.* 42.5, pp. 1406–1415.
- ⁴⁰⁵ Friston, Karl J et al. (1996). "Movement-related effects in fMRI time-series". In: *Magnetic
406 resonance in medicine* 35.3, pp. 346–355.
- ⁴⁰⁷ Gesierich, Benno et al. (2020). "Alterations and test-retest reliability of functional connec-
⁴⁰⁸ tivity network measures in cerebral small vessel disease". en. In: *Hum. Brain Mapp.*
⁴⁰⁹ 41.10, pp. 2629–2641.
- ⁴¹⁰ Glasser, Matthew F et al. (2016). "A multi-modal parcellation of human cerebral cortex".
⁴¹¹ en. In: *Nature* 536.7615, pp. 171–178.
- ⁴¹² Gordon, Evan M et al. (2016). "Generation and Evaluation of a Cortical Area Parcellation
⁴¹³ from Resting-State Correlations". en. In: *Cereb. Cortex* 26.1, pp. 288–303.
- ⁴¹⁴ Griffanti, Ludovica, Mark Jenkinson, et al. (2018). "Classification and characterization of
⁴¹⁵ periventricular and deep white matter hyperintensities on MRI: A study in older adults".
⁴¹⁶ en. In: *Neuroimage* 170, pp. 174–181.
- ⁴¹⁷ Griffanti, Ludovica, Giovanna Zamboni, et al. (2016). "BIANCA (Brain Intensity AbNormal-
⁴¹⁸ ity Classification Algorithm): A new tool for automated segmentation of white matter
⁴¹⁹ hyperintensities". en. In: *Neuroimage* 141, pp. 191–205.
- ⁴²⁰ Jagodzinski, Annika et al. (2020). "Rationale and Design of the Hamburg City Health Study".
⁴²¹ en. In: *Eur. J. Epidemiol.* 35.2, pp. 169–181.
- ⁴²² Laumann, Timothy O, Evan M Gordon, et al. (2015). "Functional system and areal organi-
⁴²³ zation of a highly sampled individual human brain". In: *Neuron* 87.3, pp. 657–670.
- ⁴²⁴ Laumann, Timothy O and Abraham Z Snyder (2021). "Brain activity is not only for thinking".
⁴²⁵ In: *Current Opinion in Behavioral Sciences* 40, pp. 130–136.
- ⁴²⁶ Laumann, Timothy O, Abraham Z Snyder, et al. (2017). "On the stability of BOLD fMRI
⁴²⁷ correlations". In: *Cerebral cortex* 27.10, pp. 4719–4732.
- ⁴²⁸ Lawrence, Andrew J, Ai Wern Chung, et al. (2014). "Structural network efficiency is as-
⁴²⁹ sociated with cognitive impairment in small-vessel disease". en. In: *Neurology* 83.4,
⁴³⁰ pp. 304–311.

- 431 Lawrence, Andrew J, Daniel J Tozer, et al. (2018). "A comparison of functional and trac-
432 tography based networks in cerebral small vessel disease". en. In: *Neuroimage Clin* 18,
433 pp. 425–432.
- 434 Lawrence, Andrew J, Eva A Zeestraten, et al. (2018). "Longitudinal decline in structural
435 networks predicts dementia in cerebral small vessel disease". en. In: *Neurology* 90.21,
436 e1898–e1910.
- 437 Macey, Paul M et al. (2004). "A method for removal of global effects from fMRI time series".
438 In: *Neuroimage* 22.1, pp. 360–366.
- 439 Makris, Nikos et al. (2006). "Decreased volume of left and total anterior insular lobule in
440 schizophrenia". In: *Schizophrenia research* 83.2-3, pp. 155–171.
- 441 Muschelli, John et al. (2014). "Reduction of motion-related artifacts in resting state fMRI
442 using aCompCor". In: *Neuroimage* 96, pp. 22–35.
- 443 Petersen, Marvin et al. (2020). "Network Localisation of White Matter Damage in Cerebral
444 Small Vessel Disease". en. In: *Sci. Rep.* 10.1, p. 9210.
- 445 Power, Jonathan D, Alexander L Cohen, et al. (2011). "Functional network organization of
446 the human brain". en. In: *Neuron* 72.4, pp. 665–678.
- 447 Power, Jonathan D, Anish Mitra, et al. (2014). "Methods to detect, characterize, and re-
448 move motion artifact in resting state fMRI". In: *Neuroimage* 84, pp. 320–341.
- 449 Prins, Niels D et al. (2005). "Cerebral small-vessel disease and decline in information pro-
450 cessing speed, executive function and memory". en. In: *Brain* 128.Pt 9, pp. 2034–2041.
- 451 Pruijm, Raimon HR et al. (2015). "ICA-AROMA: A robust ICA-based strategy for removing
452 motion artifacts from fMRI data". In: *Neuroimage* 112, pp. 267–277.
- 453 Reijmer, Yael D et al. (2016). "Small vessel disease and cognitive impairment: The rele-
454 vance of central network connections". en. In: *Hum. Brain Mapp.* 37.7, pp. 2446–2454.
- 455 Rimmele, David Leander et al. (2022). "Association of Carotid Plaque and Flow Velocity
456 With White Matter Integrity in a Middle-aged to Elderly Population". en. In: *Neurology*.
- 457 Satterthwaite, Theodore D et al. (2013). "An improved framework for confound regres-
458 sion and filtering for control of motion artifact in the preprocessing of resting-state
459 functional connectivity data". In: *Neuroimage* 64, pp. 240–256.
- 460 Schaefer, Alexander et al. (2018). "Local-Global Parcellation of the Human Cerebral Cortex
461 from Intrinsic Functional Connectivity MRI". en. In: *Cereb. Cortex* 28.9, pp. 3095–3114.

- ⁴⁶² Schlemm, Eckhard et al. (2022). "Equalization of Brain State Occupancy Accompanies
⁴⁶³ Cognitive Impairment in Cerebral Small Vessel Disease". en. In: *Biol. Psychiatry* 92.7,
⁴⁶⁴ pp. 592–602.
- ⁴⁶⁵ Schulz, Maximilian et al. (2021). "Functional connectivity changes in cerebral small vessel
⁴⁶⁶ disease - a systematic review of the resting-state MRI literature". en. In: *BMC Med.* 19.1,
⁴⁶⁷ p. 103.
- ⁴⁶⁸ Shen, Jun et al. (2020). "Network Efficiency Mediates the Relationship Between Vascular
⁴⁶⁹ Burden and Cognitive Impairment: A Diffusion Tensor Imaging Study in UK Biobank".
⁴⁷⁰ en. In: *Stroke* 51.6, pp. 1682–1689.
- ⁴⁷¹ Steegen, Sara et al. (2016). "Increasing Transparency Through a Multiverse Analysis". en.
⁴⁷² In: *Perspect. Psychol. Sci.* 11.5, pp. 702–712.
- ⁴⁷³ Sundaresan, Vaanathi et al. (2019). "Automated lesion segmentation with BIANCA: Im-
⁴⁷⁴ pact of population-level features, classification algorithm and locally adaptive thresh-
⁴⁷⁵ olding". en. In: *Neuroimage* 202, p. 116056.
- ⁴⁷⁶ Tombaugh, Tom N (2004). "Trail Making Test A and B: normative data stratified by age
⁴⁷⁷ and education". en. In: *Arch. Clin. Neuropsychol.* 19.2, pp. 203–214.
- ⁴⁷⁸ Tuladhar, Anil M, Ewoud van Dijk, et al. (2016). "Structural network connectivity and cog-
⁴⁷⁹ nition in cerebral small vessel disease". en. In: *Hum. Brain Mapp.* 37.1, pp. 300–310.
- ⁴⁸⁰ Tuladhar, Anil M, Jonathan Tay, et al. (2020). "Structural network changes in cerebral small
⁴⁸¹ vessel disease". en. In: *J. Neurol. Neurosurg. Psychiatry* 91.2, pp. 196–203.
- ⁴⁸² Tzourio-Mazoyer, Nathalie et al. (2002). "Automated anatomical labeling of activations in
⁴⁸³ SPM using a macroscopic anatomical parcellation of the MNI MRI single-subject brain".
⁴⁸⁴ In: *Neuroimage* 15.1, pp. 273–289.
- ⁴⁸⁵ Vidaurre, Diego et al. (2018). "Discovering dynamic brain networks from big data in rest
⁴⁸⁶ and task". en. In: *Neuroimage* 180.Pt B, pp. 646–656.
- ⁴⁸⁷ Wardlaw, Joanna M, Colin Smith, and Martin Dichgans (2013). "Mechanisms of sporadic
⁴⁸⁸ cerebral small vessel disease: insights from neuroimaging". en. In: *Lancet Neurol.* 12.5,
⁴⁸⁹ pp. 483–497.
- ⁴⁹⁰ Wardlaw, Joanna M, Eric E Smith, et al. (2013). "Neuroimaging standards for research
⁴⁹¹ into small vessel disease and its contribution to ageing and neurodegeneration". en.
⁴⁹² In: *Lancet Neurol.* 12.8, pp. 822–838.

- ⁴⁹³ Wardlaw, Joanna M, Maria C Valdés Hernández, and Susana Muñoz-Maniega (2015). "What
⁴⁹⁴ are white matter hyperintensities made of? Relevance to vascular cognitive impairment". en. In: *J. Am. Heart Assoc.* 4.6, p. 001140.
- ⁴⁹⁶ Xu, Yuanhang et al. (2021). "Altered Dynamic Functional Connectivity in Subcortical Is-
⁴⁹⁷ chemic Vascular Disease With Cognitive Impairment". en. In: *Front. Aging Neurosci.* 13,
⁴⁹⁸ p. 758137.
- ⁴⁹⁹ Yeo, B T Thomas et al. (2011). "The organization of the human cerebral cortex estimated
⁵⁰⁰ by intrinsic functional connectivity". en. In: *J. Neurophysiol.* 106.3, pp. 1125–1165.
- ⁵⁰¹ Yin, Wenwen et al. (2022). "The Clustering Analysis of Time Properties in Patients With
⁵⁰² Cerebral Small Vessel Disease: A Dynamic Connectivity Study". en. In: *Front. Neurol.*
⁵⁰³ 13, p. 913241.

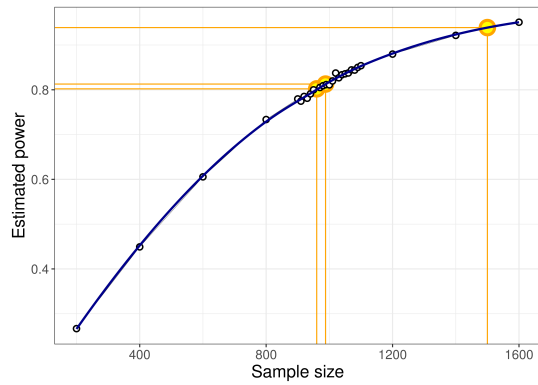


Figure 1 | Sample size and power estimation. A-priori estimated power for different sample sizes was obtained as the proportion of synthetic data sets in which the null hypothesis of no association between WMH volume and time spent in high-occupancy brain states can be rejected at the $\alpha = 0.05$ significance level. Proportions are based on a total of 10 000 synthetic data sets obtained by bootstrapping the data presented in (Schlemm et al., 2022). Highlighted in orange are the smallest sample size ensuring a power of at least 80 % ($n = 960$), the sample size of the pilot data ($n = 988$, post-hoc power 81.3 %), and the expected sample size for this replication study ($n = 1500$, a-priori power 93.9 %).

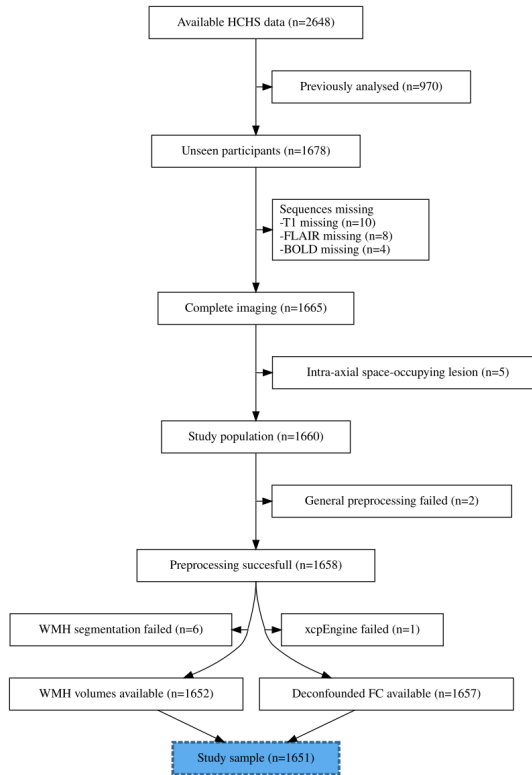


Figure 2 | Study flowchart. Composition of the study population after application of inclusion and exclusion criteria, and image processing.

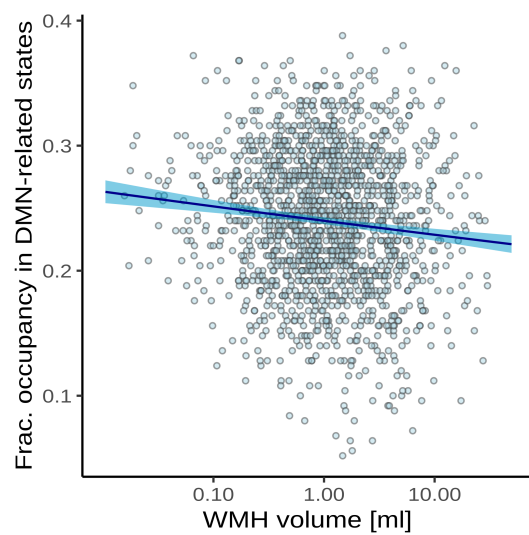


Figure 3 | Association between time spent in high-occupancy brain states and supratentorial WMH volume. Point estimates (black line) and 95%-confidence region (light blue ribbon) of the conditional mean fractional occupancy are obtained from unadjusted beta regression modelling. Each marker represents one of N=1642 independent subjects with a non-zero total WMH volume.

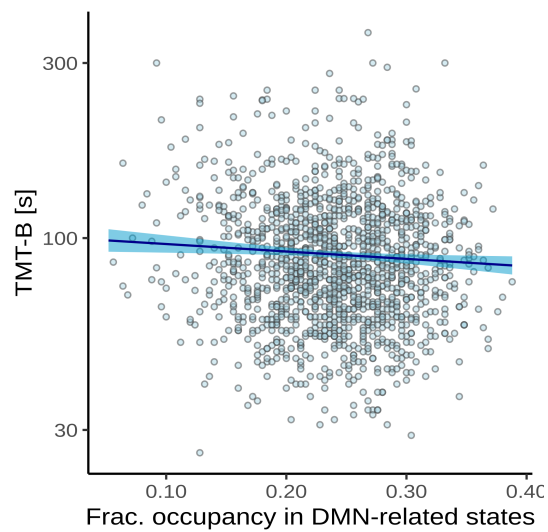


Figure 4 | Association between time spent in high-occupancy DMN-related brain states and TMT-B completion time. Point estimates (black line) and 95%-confidence region (light blue ribbon) of the conditional mean TMT-B completion time are obtained from unadjusted Gamma regression modelling. Each marker represent one of N=1482 independent subjects with non-zero total WMH volume and available TMT-B data.

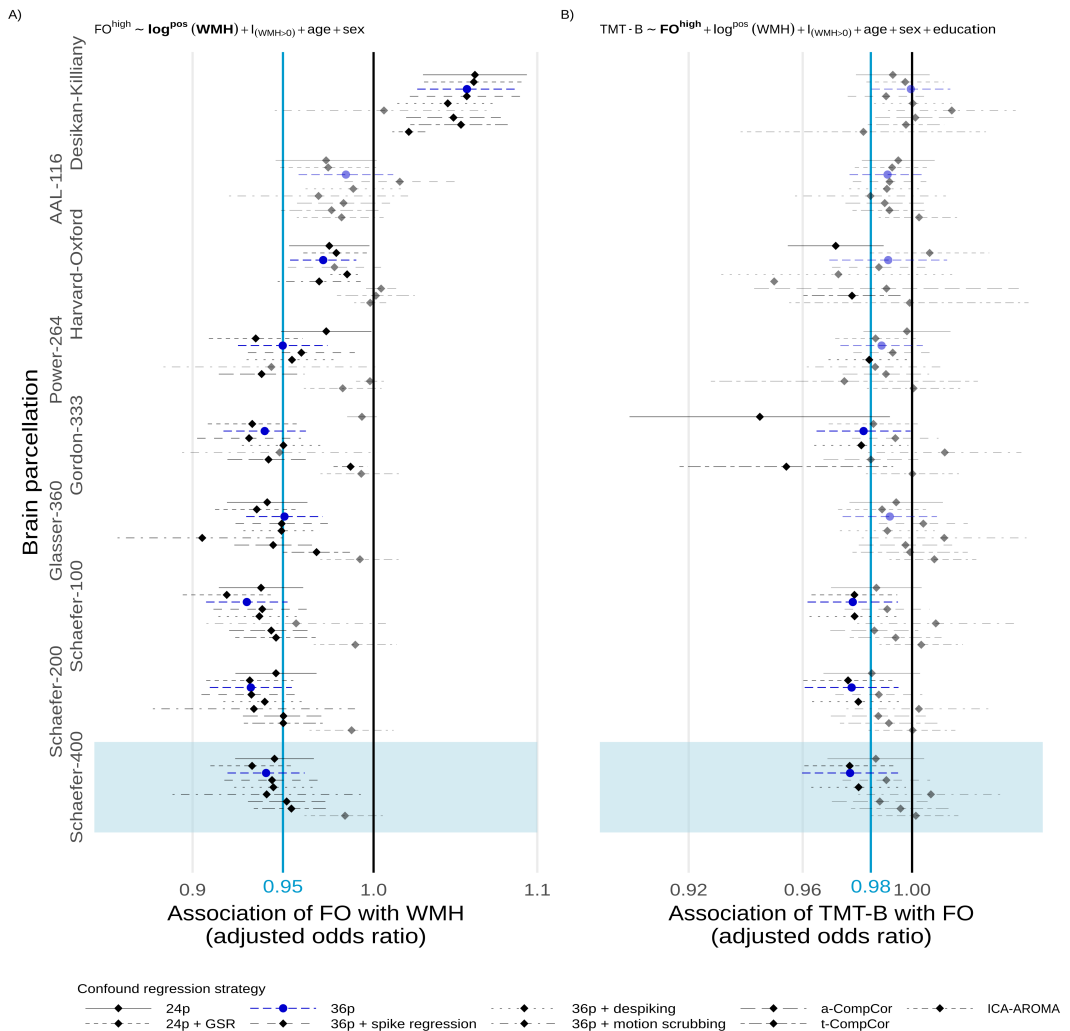


Figure 5 | Multiverse analysis. Adjusted effect size estimates of the associations between cSVD severity (WMH volume) and network dedifferentiation (less time spent in high-occupancy DMN-related brain states) [A]), and between network dedifferentiation and executive function (TMT-B completion time) [B]). Effect sizes are given per 5.1-fold increase in WMH volume and a 5%-increase in fractional occupancy, respectively. Markers and line segments indicate point estimates and 95%-confidence intervals for adjusted odds ratios for different combinations of confound regression strategy and brain parcellation. The primary analytical choices are indicated by dark blue circles (36p) and light blue shading (Schaefer-400). Model equations for beta and gamma regressions, respectively, are given at the top. Vertical lines indicate no effect (black) and the effect size observed in the discovery cohort (Schlemm et al., 2022) (light blue), respectively, for reference. Effect sizes not reaching nominal statistical significance ($\alpha = 0.05$) are shown desaturated. Corresponding data based on periventricular and deep WMH volumes are given in the Supplement.

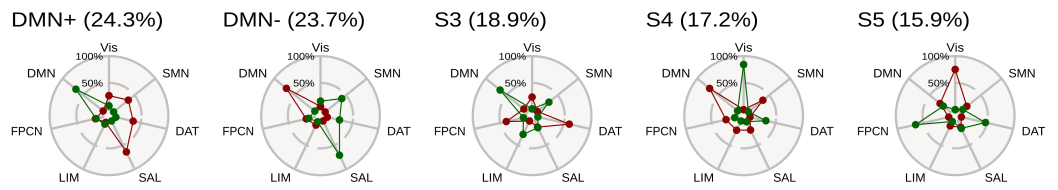


Figure 6 | Connectivity profiles of brain states. Cosine similarity between centroids of each identified brain state and signed indicator vectors corresponding to activation (green) and suppression (red) of each of seven predefined large-scale functional brain networks (Yeo et al., 2011). Parenthetical percentages indicate the mean fractional occupancy across N=1651 independent subjects. Two high-occupancy states are characterized by activation or suppression of the DMN, the remaining three low-occupancy states (S3–5) were not used in the present study.

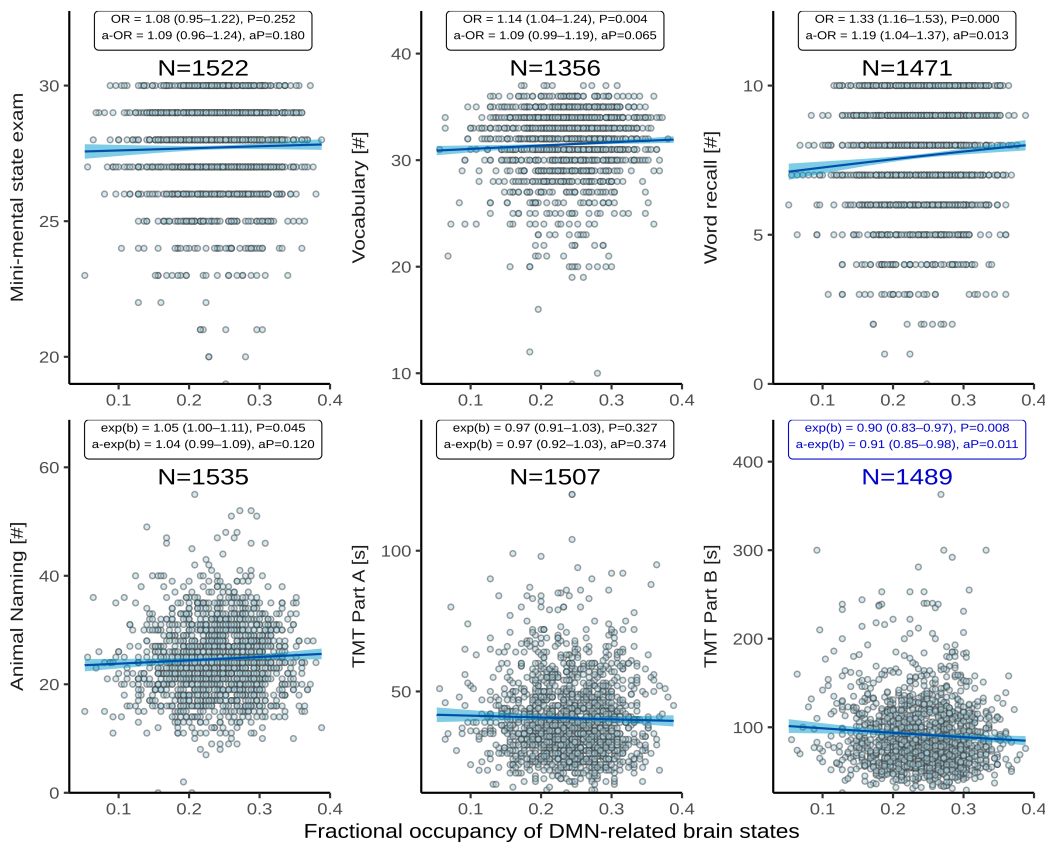


Figure 7 | Association between time spent in high-occupancy DMN-related brain states and cognitive measures. Point estimates (black line) and 95%-confidence region (light blue ribbon) of the conditional mean cognitive measures are obtained from unadjusted binomial (top row: Mini-Mental State Examination, Vocabulary, Word List Recall, logit link) and Gamma regression (bottom row: Animal Naming, Trail Making Test [TMT] A/B: log link) modelling. Each marker represents one of N independent subjects, as indicated. Insets report effect sizes and P-values both with (adjusted [a-]) and without adjustment for the nuisance variables age, sex, WMH volume (coded as in Figure 5), and years of education. Effect sizes were quantified as odds ratios (ORs) (top) or response scale multipliers [exp(b)] (bottom), and correspond to a 20%-increase in fractional occupancy. Note the different reference change in FO compared to Table 10 chosen to adequately represent some of the smaller effect sizes. The bottom right panel highlighted in dark blue reproduces Figure 4.

Question	Hypothesis	Sampling plan	Analysis plan	Rationale for deciding the sensitivity of the test	Interpretation given different outcomes	Theory that could be shown wrong by the outcome
Is severity of cerebral small disease, quantified by the volume of supratentorial white matter hyperintensities of presumed vascular origin (WMH), associated with time spent in high-occupancy brain states, defined by resting-state functional MRI?	(Primary) Higher WMH volume is associated with lower average occupancy of the two highest-occupancy brain states. (Secondary) Lower average occupancy of the two highest-occupancy brain states is associated with longer TMT-B time.	Available subjects with clinical and imaging data from the HCHS (Jagodzinski et al., 2020)	Standardized pre-processing of structural and functional MRI data • automatic quantification of WMH • co-activation pattern analysis • multivariable generalised regression analyses	Tradition	$P < 0.05 \rightarrow$ rejection of the null hypothesis of no association between cSVD and fractional occupancy; $P > 0.05 \rightarrow$ insufficient evidence to reject the null hypothesis	Functional brain dynamics are not related to subcortical ischemic vascular disease.
Is time spent in high-occupancy brain states associated with cognitive impairment, measured as the time to complete part B of the trail making test (TMT)?		as above	as above	as above	$P < 0.05 \rightarrow$ rejection of the null hypothesis of no association between fractional occupancy and cognitive impairment; $P > 0.05 \rightarrow$ insufficient evidence to reject the null hypothesis	Cognitive function is not related to MRI-derived functional brain dynamics.

Table 1 | Study Design Template. Overview of the Scientific Questions addressed in the present study (first column), the two main hypotheses being investigated (second column), and details of the underlying study.

Name of the atlas	#parcels	Reference
Desikan-Killiany	86	Desikan et al., 2006
AAL	116	Tzourio-Mazoyer et al., 2002
Harvard-Oxford	112	Makris et al., 2006
glasser360	360	Glasser et al., 2016
gordon333	333	Gordon et al., 2016
power264	264	Power, Cohen, et al., 2011
schaefer{N}	100 200 400	Schaefer et al., 2018

AAL: Automatic Anatomical Labelling

(a) Parcellations

Design	Reference
24p	Friston et al., 1996
24p + GSR	Macey et al., 2004
36p	Satterthwaite et al., 2013
36p + spike regression	Cox, 1996
36p + despiking	Satterthwaite et al., 2013
36p + scrubbing	Power, Mitra, et al., 2014
aCompCor	Muschelli et al., 2014
tCompCor	Behzadi et al., 2007
AROMA	Pruim et al., 2015

GSR: Global signal regression, AROMA: Automatic Removal of Motion Artifacts

(b) Confound regression strategies, adapted from (Ciric, Wolf, et al., 2017)

Table 2 | Multiverse analysis. Overview over different brain parcellations and confound regression strategies implemented using xcpEngine (Ciric, Rosen, et al., 2018). A total of $9 \times 9 = 81$ analytical combinations were explored to assess the robustness of our results with respect to these processing choices.

N = 1,651		
<i>Demographics (no Missing n (%))</i>		
Age	Median (IQR)	66 (59 – 72)
	Missing n (%)	
Sex	Male	940/1651 (57%)
	Female	711/1651 (43%)
<i>Cardiovascular risk factors</i>		
Hypertension	Present	1177/1611 (73.1%)
	Missing n (%)	85 (5.1%)
Diabetes	Present	157/1566 (10%)
	Missing n (%)	40 (2.4%)
Smoking	Present	200/1360 (14.7%)
	Missing n (%)	201 (12.9%)
Hyperlipidaemia	Present	426/1578 (27%)
	Missing n (%)	73 (4.4%)
<i>Cognitive test results</i>		
MMSE (#, max. 30)	Median (IQR)	28 (27 – 29)
	Missing n (%)	129 (7.8%)
Vocabulary (MWT-B) (#, max. 37)	Median (IQR)	32 (30 – 34)
	Missing n (%)	295 (18%)
Word recall #, (max. 10)	Median (IQR)	8 (6 – 9)
	Missing n (%)	180 (11%)
Animal Naming	Median (IQR)	24 (20 – 29)
	Missing n (%)	116 (7.0%)
TMT-A, seconds	Median (IQR)	38 (31 – 48)
	Missing n (%)	144 (8.7%)
TMT-B, seconds	Median (IQR)	83 (65 – 110)
	Missing n (%)	162 (9.8%)
<i>History</i>		
Diagnosed dementia	Present	6/1645 (0.4%)
	Missing n (%)	6 (0.4%)
Years of education	Median (IQR)	13 (12 – 16)
	Missing n (%)	34 (2%)

Table 4 | Descriptive statistics of the study population. Data are presented as median (interquartile range) or count (percentage) of non-missing items, as appropriate. Number of percentage of missing items are reported separately.

N = 1,651	
WMH volume ¹ , ml	
Total	1.05 (0.47 – 2.37), 9 Z
Periventricular	0.94 (0.43 – 2.04), 9 Z
Deep	0.10 (0.03 – 0.37), 344 Z
Motion during rs-fMRI	
Framewise displacement, mm	0.21 (0.15 – 0.63)
RMSD, mm	0.086 (0.058 – 0.12)
DVARS	27.8 (24.3 – 31.8)
Fractional occupancy, %	
DMN+	24.8 (20.8 – 28.0)
DMN-	24.0 (20.0 – 28.0)
S3	18.4 (15.2 – 22.4)
S4	16.8 (12.8 – 20.8)
S5	15.2 (12.0 – 19.2)

¹Number of zero values indicated by Z

Table 6 | Structural and functional imaging characteristics. Data are presented as median (interquartile range). Supratentorial WMH volumes were obtained by semiautomatic segmentation of FLAIR images using a BINACA/LOCATE-based k -nearest neighbours algorithm and stratified by their distance to the lateral ventricles (<10 mm, periventricular; >10 mm, deep). Motion parameters were estimated during fMRIprep processing of BOLD scans. Fractional occupancies were calculated by assigning individual BOLD volumes to one of five discrete brain states defined by k-means clustering-based co-activation pattern analysis.

	Estimate	P	95%-CI
Intercept	0.24	<0.0001	0.21 – 0.27
$\log \text{WMH}^+$, per 5.1-fold increase ¹	0.94	<0.0001	0.92 – 0.96
Age, per 10 years	1.04	0.001	1.01 – 1.06
Female sex	1.12	<0.0001	1.09 – 1.16
$\mathbf{1}_{\{\text{WMH}=0\}}$	0.93	0.477	0.75 – 1.14

¹ Interquartile ratio 2.37/0.468 = 5.06

Table 8 | Association between time-spent in high-occupancy DMN-related brain states and WMH adjusted for age and sex. Beta regression table estimated from $n = 1651$ independent participants using the model equation $\text{FO}^{\text{high}} \sim \log \text{WMH}^+ + \mathbf{1}_{\{\text{WMH}=0\}} + \text{age} + \text{sex}$.

	Estimate	P	95%-CI
Intercept	53.41	< 0.0001	42.7 – 66.8
FO.high, per 5%	0.98	0.0116	0.96 – 0.99
log WMH [†] , per 5.1-fold increase ¹	1.01	0.367	0.98 – 1.05
Age, per 10 years	1.18	<0.0001	1.15 – 1.21
Female sex	0.99	0.666	0.95 – 1.03
Education, per year	0.97	<0.0001	0.97 – 0.98
$\mathbf{1}_{\{\text{WMH}=0\}}$	0.97	0.398	0.92 – 1.03

¹ Interquartile ratio 2.37/0.468 = 5.06

Table 10 | Association between TMT-B and time spent in high-occupancy DMN-related brain states adjusted for age, sex, WMH volume and years of education. Gamma regression table estimated from $n = 1483$ independent participants using the model equation
 $TMT-B \sim FO^{\text{high}} + \log WMH^{\dagger} + \mathbf{1}_{\{\text{WMH}=0\}} + \text{age} + \text{sex}$